ACS OMEGA

Open Access



http://pubs.acs.org/journal/acsodf

Article

# Key Factors and Evaluation Model of Valuable Metal Separation in Low-Concentration Smelting Slag

Zhuandi Shao, Tiantian Wei, Xiujuan Zhang, Kang Liao, Xiaogang Hou, Hong Deng, Xueming Liu,* Zhang Lin, and Liyuan Chai

Cite This: *ACS Omega* 2025, 10, 9691−9702

Read Online

ACCESS | Metrics & More | Article Recommendations | Supporting Information

**ABSTRACT:** The low concentration of valuable metals in smelting slags poses a significant challenge for separation. Despite the effective separation achieved by current pyrometallurgical or hydrometallurgical methods, the intricate mineralogy of slag and numerous leaching factors present considerable challenges in selecting the appropriate separation techniques and parameters for efficient and rapid extraction. In this study, copper slag flotation tailings (CSFT) were taken as an example, and the microexistence forms of valuable metals were analyzed through XRD and SEM-EDS. By integrating theoretical calculations and TGA analysis, a method involving concentrated sulfuric acid roasting and subsequent water leaching was employed to sufficiently extract valuable metals Mg, Cu, and Ni, concurrently achieving depth separation from Fe in the slag. Concurrently, a dynamic evaluation model correlating metal leaching efficiency ($X_t$) with key factors has been established, enabling the quantification of valuable metal leaching performance under various conditions. Based on the kinetics equation and Arrhenius formula, with roasting temperature ($T$), roasting time ($t$), acid-to-solid ratio ($r$), and particle size ($d$) as key parameters, using experimental data, a dynamic evaluation model with kinetic characteristics was established as follows: $1/3\ln(1-X_t) - [1-(1-X_t)^{-1/3}] = 9.36r^{1.55}d^{-1.40}e^{-21957.8/RT}t$. The influence order was determined as roasting temperature > acid-to-solid ratio > particle size. The simulated values closely matched the experimental values, allowing the model to accurately predict the metal leaching rates. This provides an essential method for the design of metal recovery reaction parameters and optimization of engineering outcomes in the treatment of smelting slag.

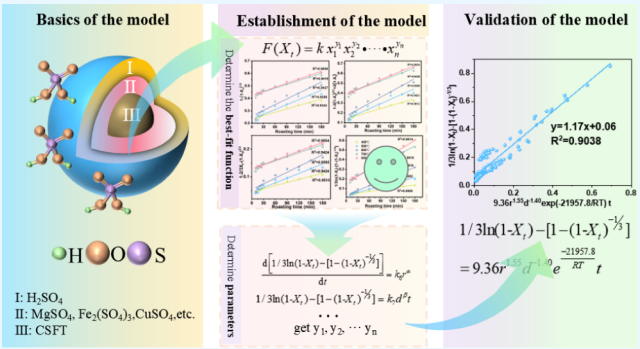


## 1. INTRODUCTION

The annual emission of smelting slag in China exceeds 30 million tons, yet its utilization remains low, resulting in an exponential increase in stockpiles.[1] This phenomenon not only occupies significant land resources but also severely pollutes water and soil, while additionally leading to the waste of valuable metals.[2−4] The resource utilization of smelting slag is an urgent requirement for the green development of industries such as chemicals and steel in China, serving as a primary means to address the issue of substantial stockpiles. The efficient recovery of valuable metals from smelting slag is one effective approach to resource utilization. Current methodologies for metal recovery primarily encompass pyrometallurgical, hydrometallurgical, and combined pyro-hydrometallurgical techniques.[5−7] Pyrometallurgy, recognized for its rapid enrichment of valuable metals and robust adaptability to various feedstocks, is extensively utilized for the efficient processing of large volumes of smelting slag.[8,9] However, pyrometallurgy also has drawbacks, such as high energy consumption and environmental unfriendliness. Additionally, from the perspective of slag composition, pyrometallurgy requires relatively high contents of Fe[10−12] and valuable metals, such as Cu,[13] Ni,[8,14] and Zn,[15] to effectively concentrate and recover these metals through pyrometallurgical methods. In contrast to pyrometallurgy, hydrometallurgy offers lower energy consumption and higher recovery rates of valuable metals.[16] However, the adaptability of hydrometallurgy to various raw materials is relatively poor, and the presence of iron in slag poses a particularly challenging issue. After leaching, the excessive iron in the solution makes the subsequent handling of the leaching solution more complex.[17] Overall, the presence of valuable metals in smelting slag, characterized by low concentrations, diverse varieties, and complex phases, complicates efficient and economical enrichment through pyrometallurgical or hydrometallurgical methods

**Received:** December 10, 2024
**Revised:** February 12, 2025
**Accepted:** February 14, 2025
**Published:** March 1, 2025

alone. The integrated pyrohydrometallurgical process, involving sulfuric acid or sulfate activation roasting followed by water leaching, distinguishes itself by addressing these issues. Adding sulfuric acid,[18] sodium sulfate,[19,20] or ammonium sulfate[21,22] in appropriate amounts during slag roasting facilitates the leaching of valuable metals into soluble phases, thereby segregating them from iron and other residues. Given this, the pyro-hydro method is widely used in the recovery of metals from slag.

The extraction of valuable metals is influenced by various factors, such as additive quantities, particle size of slag, roasting conditions, leaching parameters, and pH,[23−25] with roasting temperature, time, additive amount, and particle size being pivotal in integrated pyrometallurgical and hydrometallurgical processes.[9,26] Combined with the preliminary experiments shown in Figure S1a−c, under certain conditions, the influence of water-leaching conditions on the leaching effect is not particularly significant. Therefore, this study focused on the analysis of the influencing factors in the roasting process, which have a significant impact on metal extraction. Current research is case-specific and lacks comprehensive assessment, focusing on various factors affecting leaching outcomes for different slags. There is an urgent need to establish a dynamic evaluation model to systematically assess the main factors influencing metal extraction, thereby guiding efficient recovery and process optimization.

Assessment methods focus on leaching kinetics of smelting slag, typically utilizing the unreacted shrinking core model for solid−liquid or solid−liquid−gas heterogeneous systems. By calculating the activation energy of the reaction, the resistance of the leaching process can be assessed, indicating whether it is controlled by diffusion or interface reactions.[27−29] The impact of critical factors on the experimental procedure has not been quantified. Some studies have refined the apparent rate constant $k$ in the unreacted shrinking core model, introducing factors closely related to the leaching rate, such as additive concentration and smelting slag particle size, which have better expressed the impact of these factors on leaching results.

However, the order of additive concentration is roughly regarded as first order or $n$-th order, and the order of reactant particle size is regarded as negative one or negative two by these models, which still cannot thoroughly indicate the influence of each key factor on the metal leaching rate.[30−32] First, the unreacted shrinking core model is employed to establish a function $F(X_t)$ correlated with the leaching rate via experimental means. Subsequently, the apparent rate constant $k$ is modeled as a function of critical factors influencing metal leaching, with their influence quantified by exponents $x_1^{y_1}x_2^{y_2}\cdots\cdots x_n^{y_n}$. These exponents are determined empirically to evaluate the factors' impact on metal extraction. The resulting expression is presented in eq 1. Finally, the experimental data are regressed against the model to assess the fit.

$$F(X_t) = kt \tag{1}$$

where $F(X_t)$ represents the function correlated with the leaching rate; $k$ represents the apparent rate constant ( $k = k_0x_1^{y_1}x_2^{y_2}\cdots\cdots x_n^{y_n}$); $k_0$ represents the coefficient of the apparent rate constant in relation to various influencing factors; $x_1$, $x_2$, ..., $x_n$ represent the key factors affecting the recovery of the valuable metals; $y_1$, $y_2$, ..., $y_n$ represent the exponents of the influencing factors.

In this study, copper slag flotation tailings were utilized as a case study. A method involving concentrated sulfuric acid roasting and subsequent water leaching was employed to extract valuable metals Mg, Cu, and Ni. Additionally, focusing on Mg, which is abundant in CSFT, a kinetic model was developed to establish the model between Mg leaching efficiency and roasting temperature, the original slag particle size, and sulfuric acid dosage. Experimental data were employed to validate the model's predictive accuracy. The study comprises (1) the analytical identification of the micromorphology of key elements in CSFT; (2) the analysis of critical factors impacting the leaching of valuable metals via integrated sulfuric acid roasting; and (3) the construction of an evaluative model for Mg extraction as influenced by key factors.

## 2. MATERIALS AND METHODS

**2.1. Experimental Materials.** CSFT originate from Northwest China. The slag utilized in the experiments was dried at 60 °C for 24 h, followed by grinding and sieving. Sulfuric acid ($H_2SO_4$, AR, molecular weight is 98.08 wt %) was purchased from Guangzhou Chemical Reagent Factory (China). $HNO_3$, HCl, and $H_2O_2$ were acquired from Shanghai Macklin Biochemical Co. Ltd. (Shanghai, China). All chemicals used in this study were of analytical grade. The experimental water was deionized.

**2.2. Experimental Methods and Procedures.** *2.2.1. Determination of Metal Content in CSFT.* The metal elements in CSFT were analyzed using X-ray fluorescence spectroscopy (XRF, ZSX Primus II, Rigaku, Japan). Concentrations of metal elements in CSFT were tested using inductively coupled plasma optical emission spectrometry (ICP-OES, Avio 200, PerkinElmer, USA). The procedure is as follows: accurately weigh a sample and add 6 mL $HNO_3$, 0.5 mL HF, 2 mL $H_2O_2$, and 1 mL HCl, then heat at 210 °C for 8 h to fully digest before analysis.

*2.2.2. Leaching Experiment of Valuable Metals.* In this study, a concentrated sulfuric acid roasting and subsequent water leaching process was employed to extract valuable metals Mg, Cu, and Ni, concurrently achieving separation from Fe in the slag. First, 1 g of pretreated primary slag with varying particle sizes (74 $\mu$m, 110 $\mu$m, and 180 $\mu$m) was thoroughly mixed with sulfuric acid in different ratios (0.6−1.8 mL). Second, the mixture was roasted in an air atmosphere at specific temperatures (400−800 °C) for durations ranging from 10 to 180 min, with a controlled heating and cooling rate of 10 °C $min^{-1}$. Third, after cooling the roasted slag to room temperature, it was mixed with 10 mL of deionized water and leached at 200 rpm and 60 °C for 1 h. During the leaching process, valuable metals Mg, Cu, and Ni were dissolved in the leaching solution. Finally, the subsequent solid−liquid mixture obtained from leaching was centrifuged at 9000 rpm for 1 min to separate the solution containing the valuable metals from the iron-rich leach residue. The recovery rate of valuable metals was calculated using eqs 2 and 3.

$$M_i = C_i \times V \tag{2}$$

$$\eta_i = \frac{M_i}{M_{i0}} \times 100 \tag{3}$$

where $M_i$ represents the mass of each metal (mg), $C_i$ represents the concentration of each metal in the leaching solution (mg/L), $V$ represents the volume of the leaching solution (L), $\eta_i$



https://doi.org/10.1021/acsomega.4c10942
ACS Omega 2025, 10, 9691−9702

**Table 1. Content of Major Elements in CSFT**

| Element | Si | Mg | Fe | Ca | Al | Na | Cu | Ni |
|---|---|---|---|---|---|---|---|---|
| Content ($mg \cdot g^{-1}$) | 257.31 | 142.50 | 90.01 | 32.85 | 20.66 | 13.07 | 1.40 | 1.10 |

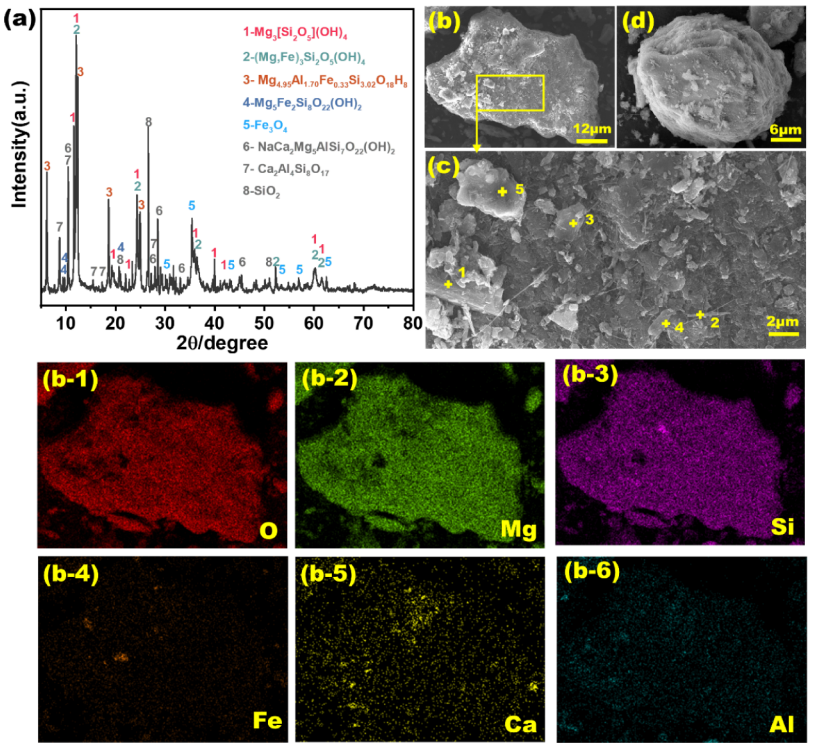


**Figure 1.** Microscopic distribution of valuable metals in the CSFT. (a) XRD spectrum; (b) (d) SEM secondary electron images; (b-1)−(b-6) Important elements mapping images; (c) local magnification of complex regions in the image.

represents the leaching rate of each metal, and $M_{i0}$ represents the mass of each metal in the original residue (mg).

*2.2.3. Leaching Evaluation Model of Mg.* First, to quantitatively examine the effect of roasting temperature on Mg leaching efficiency, 1 g of pretreated slag mixed with concentrated sulfuric acid was roasted at 400, 500, 600, 700, and 800 °C for varying durations (10−180 min), employing the optimal acid-to-solid ratio and particle size outlined in Section 2.2.2. Aqueous leaching was then conducted to establish the relationship between the Mg leaching efficiency and roasting time at these temperatures. Second, to quantitatively investigate the effect of acid-to-solid ratio on Mg leaching efficiency, 1 g of pretreated slag mixed with concentrated sulfuric acid was roasted at various acid-to-solid ratios of 0.6, 1.0, 1.2, 1.4, and 1.8 (mL:g) for durations (10−180 min), following the optimal temperature and particle size. Subsequent leaching determined the relationship between the Mg leaching efficiency and roasting time at these ratios. Third, to quantitatively investigate the effect of particle size of the original slag on Mg leaching efficiency, 1 g of pretreated slag mixed with concentrated sulfuric acid was roasted at different particle sizes of 74, 110, and 180 ($\mu$m) for durations (10−180 min), using the optimal temperature and acid-to-solid ratio. Aqueous leaching was then performed to determine the relationship between the Mg leaching efficiency and time at these varying particle sizes. The heating rate in the tube furnace and the aqueous leaching conditions are identical to those described in Section 2.2.2.

**2.3. Analysis and Characterization Methods.** The metal elements in CSFT were analyzed using X-ray fluorescence spectroscopy (XRF, ZSX Primus II, Rigaku, Japan). The concentrations of metal elements in CSFT and leaching solution were determined by inductively coupled plasma-atomic emission spectrometry (ICP-OES, Avio 200, PerkinElmer, USA). The phase composition of the samples, roasted residues, and leached residues was examined by an X-ray diffractometer (XRD, Bruker, Germany) using Cu K$\alpha$ radiation, a tube voltage of 40 kV, a tube current of 40 mA, and a scanning step of 0.02°. The microstructure, morphology, and elemental analysis of the samples and leach residues were examined using a field emission scanning electron microscope equipped with energy dispersive X-ray spectroscopy (SEM-EDS, TESCAN MIRA LMS, Czechia) at an accelerating voltage of 10 kV. Weight loss analysis of the samples in concentrated sulfuric acid was conducted using a thermal gravimetric analyzer (TGA, Mettler, Switzerland), under an oxygen atmosphere, with a temperature range of 30−1200 °C and a heating rate of 10 °C/min. The specific surface area of raw ore samples with varying particle sizes was analyzed using an accelerated surface and porosimetry system (BET, Micromeritics ASAP2460, USA). The Gibbs free energy ($\Delta G^{\circ}$) of the relevant reactions was calculated using HSC Chemistry 6.0.

## 3. RESULTS AND DISCUSSION

**3.1. Microscopic Distribution of Valuable Metals in CSFT.** Based on the qualitative analysis of XRF in Table S1, we employed the digestion method described in Section 2.2.1 for



https://doi.org/10.1021/acsomega.4c10942
ACS Omega 2025, 10, 9691−9702

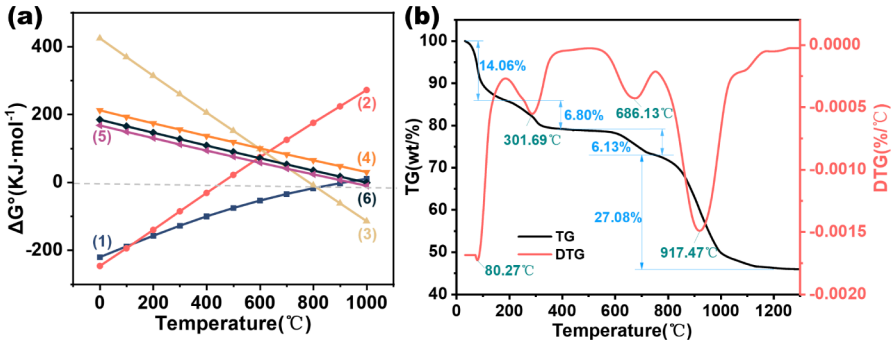


**Figure 2.** Reaction between CSFT and concentrated sulfuric acid. (a) the Gibbs free energy ($\Delta G^\circ$) diagrams of the reaction equations at different temperatures; (b) the TG-DTG curve under an air atmosphere with a heating rate of 10 °C $min^{-1}$.

the quantitative analysis of element contents in CSFT, as shown in Table 1. The digestion results indicated that CSFT contain the highest concentration of Si (approximately 260 $mg{\cdot}g^{-1}$), followed by Mg and Fe (about 142 $mg{\cdot}g^{-1}$ and 90 $mg{\cdot}g^{-1}$, respectively). The concentrations of Cu and Ni were 1.40 $mg{\cdot}g^{-1}$ and 1.10 $mg{\cdot}g^{-1}$, respectively.

To further investigate the phase composition of the CSFT, a phase analysis was performed using XRD, as shown in Figure 1a . The main phases of CSFT include lizardite-1T [$Mg_3[Si_2O_5](OH)_4$], lizardite-1 M [$(Mg,Fe)_3Si_2O_5(OH)_4$], anthophyllite [$Mg_5Fe_2Si_8O_{22}(OH)_2$)], and clinochlore ($Mg_{4.95}Al_{1.70}Fe_{0.33}Si_{3.02}O_{18}H_8$), where Mg is partially substituted by Fe or Al. Other minerals present include edenite and partheite. Besides these silicate minerals, the slag also contains magnetite, which contributes to its strong magnetic properties.

SEM-EDS analysis was utilized to further elucidate the micromorphology of the slag and its elemental associations. As shown in Figure 1b,d, CSFT is primarily composed of blocky and irregularly layered spherical particles. Local magnification of complex regions with blocky surface morphology, as shown in Figure 1c, reveals the presence of various substances, including cylindrical, rod-like, layered, and flaky materials. Atomic ratio analysis, as illustrated in Figure S2, indicated that cylindrical phase 1 (Figure S2a) could be reasonably deduced as $Mg_5Fe_2Si_8O_{22}(OH)_2$. In contrast, the rod-like phase 2, layered phase 3, and flaky phase 4 (Figure S2b−d) were postulated to be $Mg_3[Si_2O_5](OH)_4$. Moreover, the element distribution map (Figure 1b-4) validates that the Fe-rich flaky phase 5 (Figure S2e) could be hypothesized as $Fe_3O_4$. In addition, elemental mapping and atomic ratio analysis of Figure S3 suggested that the irregularly layered spherical phase could be speculated to be $(Mg,Fe)_3Si_2O_5(OH)_4$. Notably, these inferences were in excellent agreement with the aforementioned XRD analysis.

Hence, it was evident that CSFT contained a multitude of elements and complex phases, with valuable metal Mg present in insoluble silicate phases. Cu and Ni were associated with Si or Fe, forming silicate or ferrite phases rather than independent phases within the slag.[33] Additionally, Fe, which needs to be removed, could combine with the Mg required for leaching to form Mg−Fe or Mg−Fe−Al silicate minerals. This presented the main challenge of how to effectively extract Mg, Cu, and Ni while achieving efficient removal of the impurity Fe.

**3.2. The Impact of Concentrated Sulfuric Acid Roasting on Metal Separation.** Initially, the theoretical Gibbs free energy profiles for the reactions of major phases with concentrated sulfuric acid were calculated using HSC Chemistry 6.0, as depicted in Figure 2a, with the reaction equations provided in Table 2. The calculation results indicated that the reaction (1) between the magnesian silicate phase, represented by lizardite-1T and concentrated sulfuric acid, could occur at room temperature. Similarly, the reaction (2) involving magnetite could proceed under certain conditions. However, as the temperature increased, Gibbs free energy $\Delta G^\circ>0$ for both reactions, indicating that high temperatures could affect the reaction progress. Additionally, the decomposition reactions of $Fe_2(SO_4)_3$ as shown in reaction (3) and three other sulfates in reactions (4), (5), and (6) occur at distinctly different temperatures when the Gibbs free energy $\Delta G^\circ<0$.

**Table 2. Reaction Equations of Different Phases with Concentrated Sulfuric Acid**

| | |
|---|---|
| $Mg_3Si_2O_5(OH)_4 + 3H_2SO_4$ (l) = $3MgSO_4 + 2SiO_2 + 5H_2O$ (l) | (1) |
| $Fe_3O_4 + 4H_2SO_4$ (l) = $FeSO_4 + Fe_2(SO_4)_3 + 4H_2O$ (l) | (2) |
| $Fe_2(SO_4)_3 = Fe_2O_3 + 3SO_3$ (g) | (3) |
| $MgSO_4 = MgO + SO_3$ (g) | (4) |
| $NiSO_4 = NiO + SO_3$ (g) | (5) |
| $CuSO_4 = CuO + SO_3$ (g) | (6) |

This suggests that the selective extraction of valuable metals Mg, Cu, and Ni can be achieved by controlling the roasting temperature to decompose different sulfates. Furthermore, the decomposition temperature of $Fe_2(SO_4)_3$ is approximately 480 °C, while those of $CuSO_4$ and $NiSO_4$ are around 600 and 700 °C,[34] respectively. In contrast, $MgSO_4$ decomposes at about 890 °C.[35] This further demonstrates the feasibility of separating Mg, Cu, Ni, and Fe by controlling the roasting temperature. However, due to the complexity of the smelting slag phases and the interplay between them, there is a certain discrepancy between the theoretical and the actual decomposition temperature.[36] Consequently, thermogravimetric (TG) experiments were conducted on the reaction of CSFT with concentrated sulfuric acid (with a liquid-to-solid ratio of 1.2 mL/g), and the TG-DTG curves, as shown in Figure 2b , were obtained. The figure reveals four distinct weight loss stages throughout the heating process. The initial weight loss up to 400 °C is attributed to the volatilization of excess sulfuric acid and the loss of free and bound water in $MgSO_4$ ($H_2O$) and $FeSO_4$ ($H_2O$). The subsequent weight loss from 400 to 750 °C is predominantly due to the decomposition of sulfates, including $Fe_2(SO_4)_3$. Beyond 750 °C, the substantial weight loss is likely a result of the decomposition of newly formed substances, such as actinolite and $MgSO_4$, produced in the reaction between CSFT and sulfuric acid. Thus, a concentrated


https://doi.org/10.1021/acsomega.4c10942
ACS Omega 2025, 10, 9691−9702

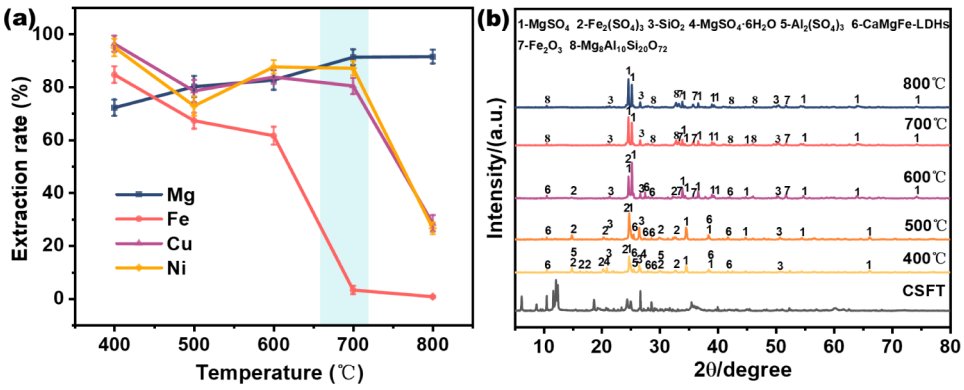


**Figure 3.** (a) Leaching rates of Mg, Fe, Cu, and Ni at different temperatures; (b) XRD spectra of the roasted slag at different temperatures under optimal conditions.

sulfuric acid roasting method with temperature control was adopted to convert Mg to soluble $MgSO_4$ and Fe to insoluble $Fe_2O_3$, while entrapped or interspersed Cu and Ni were released from the silicate phases. Finally, achieving the selective extraction and separation of valuable metals Mg, Cu, and Ni from Fe is theoretically viable.

**3.3. Analysis of Key Factors Affecting the Separation of Valuable Metals.** *3.3.1. Effect of Roasting Temperature.* The influence of temperature on the leaching of various metals was investigated at an acid-to-solid ratio of 1.2:1, a roasting time of 120 min, and a particle size of 74 $\mu$m. As shown in Figure 3a, the Mg leaching rate increases with temperature, reaching about 91% at 700 °C and then stabilizing. This finding implies that elevated temperatures enhance the sulfate's ability to decompose magnesium-rich silicate phases, thereby facilitating the thorough release of Mg. The leaching rates of Cu and Ni exceeded 90% at 400 °C but fell below 80% by 500 °C. This reduction occurs before reaching the decomposition temperatures of $CuSO_4$ and $NiSO_4$, likely due to the incorporation of Cu and Ni into CaMgFe-layered double hydroxides (LDHs) at 500 °C. At 700 °C, the leaching rates for Cu and Ni were approximately 80% and 87%, respectively. Above 700 °C, the rapid decrease in their leaching rates was attributed to the decomposition of their sulfates. The leaching rate of Fe exceeded 80% at 400 °C. The concentration of Fe in the leaching solution gradually decreased as the temperature increased. By 700 °C, the Fe content dropped to approximately 3%. At 800 °C, Fe was nearly absent. Notably, the energy consumption at 700 °C is relatively low. Therefore, the optimal roasting temperature was determined to be 700 °C.

The XRD spectra of the roasted slag at different temperatures are shown in Figure 3b. First, at 400 °C, the phases in CSFT were attacked and reacted with concentrated sulfuric acid directly to form soluble sulfates such as $MgSO_4$, $Fe_2(SO_4)_3$, which was also the reason why the leaching rates of Mg and Fe were relatively high at this temperature (Figure 3a). Second, for Mg, CaMgFe-LDHs[37] were formed by the recombination of elements such as Ca, Mg, and Fe with the Si−O structure between 400 and 600 °C, which was the main reason for the reduced Mg leaching rate in this temperature range. For Fe, as known from Section 3.2, the decomposition temperature of $Fe_2(SO_4)_3$ is approximately 480 °C. Therefore, within this temperature interval, not only did the formation of CaMgFe-LDHs lead to the decrease in the Fe leaching rate but also the decomposition of $Fe_2(SO_4)_3$ was the main cause of it. Third, at 700 °C for Mg, the LDHs structure collapsed due to excessive temperature. In addition, the large ionic radius of $Ca^{2+}$ yields unstable complexes with $Mg^{2+}$, prompting $Mg^{2+}$ to selectively form cordierite ($Mg_8Al_{10}Si_{20}O_{72}$) alongside $Al^{3+}$ due to their comparable ionic radius.[38] The stable structure of cordierite ensured its persistence even when the temperature was raised to 800 °C, which was also the reason why Mg could not be completely leached. At the same time, $Fe_2(SO_4)_3$ was completely decomposed into $Fe_2O_3$, and this temperature was far beyond 480 °C. This discrepancy could be attributed to the influence of complex mineral compositions and chemical constituents.[36] In addition, for Si, as shown in Figure 3b, it existed in three forms ($SiO_2$, CaMgFe-LDHs, and $Mg_8Al_{10}Si_{20}O_{72}$), all of which were insoluble in water, thus enabling its good separation from Mg and other elements. Finally, for Cu and Ni, due to their low concentrations, the diffraction peaks of Cu and Ni were not observable in the XRD spectrum. However, based on the above analysis, we speculated that Cu and Ni were first fully released by concentrated sulfuric acid breaking down the silicate phases. Correspondingly, sulfates of Cu and Ni were formed during the roasting process as well. Moreover, at 500 °C, the leaching rates of Cu and Ni experienced a decline, whereas at 600 °C, they continued to increase. As shown in Figure 3b, this behavior could likely be ascribed to the formation of CaMgFe-LDHs precisely at 500 °C, leading to the secondary doping or entrapment of Cu and Ni. Furthermore, a precipitous decline was witnessed in the leaching rates of Cu and Ni when the temperature ascended beyond 700 °C. As known from Section 3.2, $CuSO_4$ and $NiSO_4$ decomposed into water-insoluble oxides at this temperature. Therefore, it was postulated that the sulfates of Cu and Ni would also decompose accordingly, thereby leading to a sharp decrease in their leaching rates.

*3.3.2. Effect of Acid-to-Solid Ratio.* The influence of the acid-to-solid ratio on the leaching rates of various metals was investigated at a roasting temperature of 700 °C, a roasting time of 120 min, and a particle size of 74 $\mu$m. As shown in Figure 4, the leaching rates of Mg, Cu, and Ni reached their maxima at an acid-to-solid ratio of 1.2. When the acid-to-solid ratio was less than 1.2, the lower leaching rates of Mg, Cu, and Ni might be attributed to insufficient sulfuric acid to adequately disrupt the structure of the CSFT, further indicating that Cu and Ni are entrapped or interspersed within the silicate phases. When the acid-to-solid ratio surpassed 1.2, the leaching rate of Mg stabilized, whereas that of Cu and Ni exhibited a decline. This phenomenon might


https://doi.org/10.1021/acsomega.4c10942
ACS Omega 2025, 10, 9691−9702

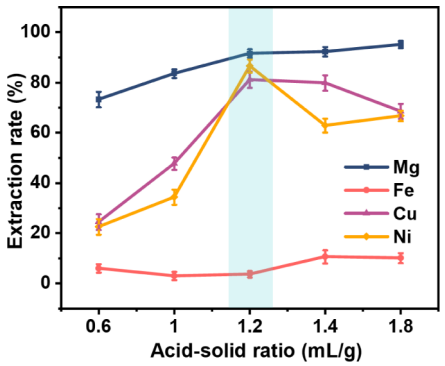


**Figure 4.** Leaching rates of Mg, Fe, Cu, and Ni at different acid-to-solid ratios.

be attributed to an excess of sulfuric acid encapsulating the roasted slag's surface, leading to the re-encapsulation of Cu and Ni, which were released from silicate phases, into newly formed phases such as cordierite. At acid-to-solid ratios ranging from 0.6 to 1.2, Fe leaching was minimal; however, when the ratio exceeded 1.2, the leaching rate of Fe reached 10%, which indicated that an excess of sulfuric acid dissolves $Fe_2O_3$. Therefore, the optimal acid-to-solid ratio was determined to be 1.2:1.

*3.3.3. Effect of Roasting Time.* The influence of roasting time on the leaching of various metals was examined at a roasting temperature of 700 °C, an acid-to-solid ratio of 1.2:1, and a particle size of 74 $\mu$m. As depicted in Figure 5, an

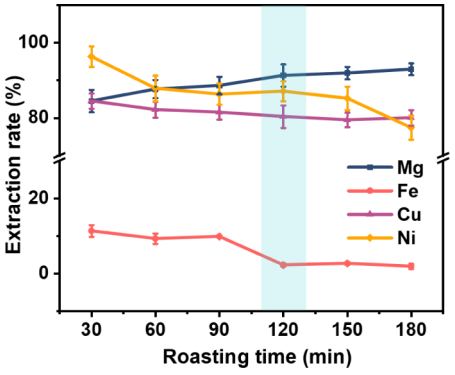


**Figure 5.** Leaching rates of Mg, Fe, Cu, and Ni at different roasting times.

increase in the roasting time allowed for a more complete reaction, consequently enhancing the leaching rate of Mg with a prolonged roasting duration. However, the leaching rates of Cu and Ni declined with reaction time, dropping to approximately 80% after 180 min, potentially due to the decomposition of $CuSO_4$ and $NiSO_4$ as the roasting time increased. The leaching rate of Fe was lowest at 120 min, with further increased roasting time causing little change in the leaching rate. Therefore, the optimal roasting time was determined to be 120 min.

*3.3.4. Effect of the Original Slag Particle Size.* The influence of CSFT particle size on the leaching of various valuable metals was investigated at a roasting temperature of 700 °C, an acid-to-solid ratio of 1.2:1, and a roasting time of 120 min. As depicted in Figure 6, the leaching rates of Mg, Cu, and Ni were highest at a particle size of 74 $\mu$m and declined with increasing particle size. This outcome was primarily

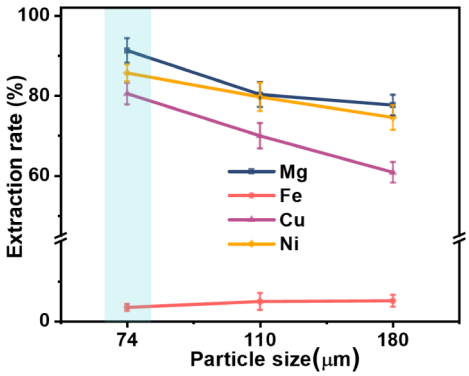


**Figure 6.** Leaching rates of Mg, Fe, Cu, and Ni at different particle sizes of the original slag.

attributed to smaller CSFT particles having a larger surface area, as shown in Table S2, leading to a greater contact area with sulfuric acid and more complete reactions. The leaching rates of Fe were consistently low, with particle size variations having negligible effects on the leaching rates. Therefore, the optimal particle size was determined to be 74 $\mu$m.

*3.3.5. Analysis of Leaching Results.* Based on the aforementioned findings, the optimal roasting conditions were established as follows: a roasting temperature of 700 °C, an acid-to-solid ratio of 1.2:1, a roasting time of 120 min, and a CSFT particle size of 74 $\mu$m. As shown in Figure 7a, after the optimal treatment of 1 g of the original slag, the compositions of the leaching solution and residue were as follows: Mg, Cu, and Ni were almost entirely leached out, while Fe remained in the leaching residue (the notation $mg \cdot g^{-1}$ indicated the mass of each element in the leaching solution and residue obtained from 1 g of the original slag). Fe and Si were almost entirely present in the leach residue, which was conducive to downstream recovery processes. The XRD spectrum of the leach residue was presented in Figure 7b, evidently showing that Fe was primarily present in $Fe_2O_3$ and $Ca_2(Mg,Fe_2)_5Si_8O_{22}(OH)_2$, both of which are water-insoluble phases, resulting in the selective removal of Fe from the leaching solution. In addition, for Si, as shown in Figure 7b, it exists in three forms ($SiO_2$, $Ca_2(Mg,Fe_2)_5Si_8O_{22}(OH)_2$, and $Mg_2Si_2O_6$) after water leaching. These silicon-containing phases are all insoluble in water, so almost all of the silicon remained in the water leaching slag. The SEM-EDS image of the leach residue is shown in Figure 7c, revealing that the residue is primarily composed of blocky and flocculent materials. Elemental mapping indicates that the main elements were Fe and Si in the leach residue, which was consistent with the analysis from ICP-OES results. Three analytical results indicated that Mg, Cu, and Ni from CSFT could be almost completely extracted and separated from Fe using concentrated sulfuric acid roasting and subsequent water leaching process.

**3.4. Development of a Mg Leaching Evaluation Model with Kinetic Characteristics.** *3.4.1. Establishment of the Optimal Function $F(X_t)$.* The leaching of the major element Mg was focused on, and an evaluation model that correlated the roasting temperature, acid-to-solid ratio, and particle size of the original slag to the Mg leaching efficiency was established. Let the function related to the leaching rate be denoted as $y = F(X_t)$. From the aforementioned analysis, it could be inferred that CSFT possessed a dense structure, essentially resembling a pore-free particle, which was gradually


https://doi.org/10.1021/acsomega.4c10942
ACS Omega 2025, 10, 9691−9702

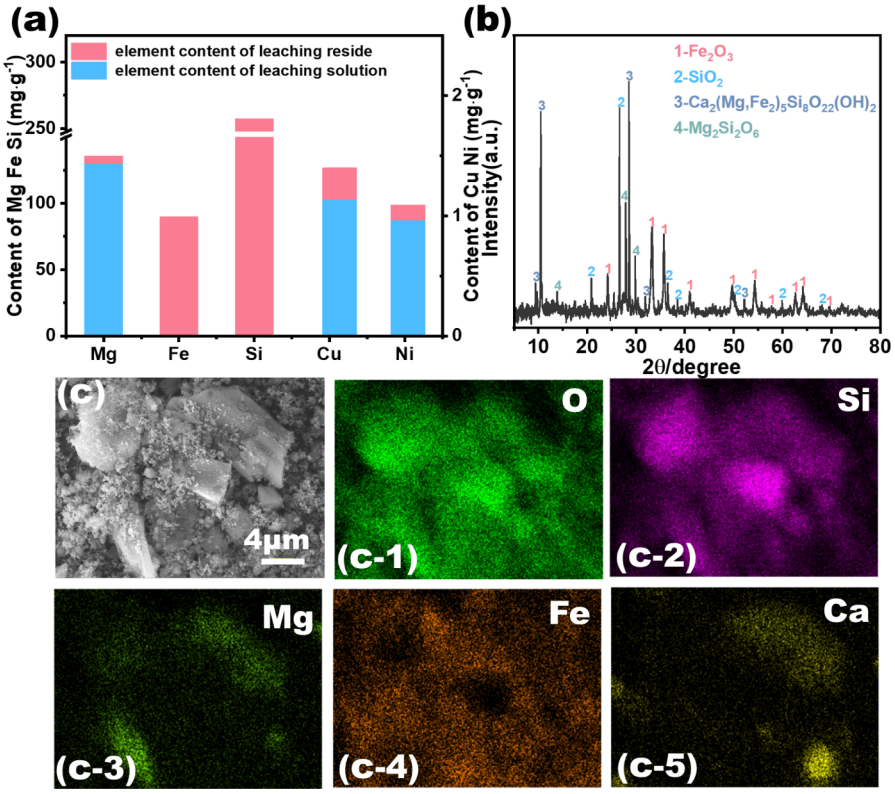


**Figure 7.** Basic information on water leaching solution and residue. (a) Elemental content in the leaching solution and residue; (b) XRD spectrum of leaching residue; (c) SEM secondary electron images, important element mapping images.

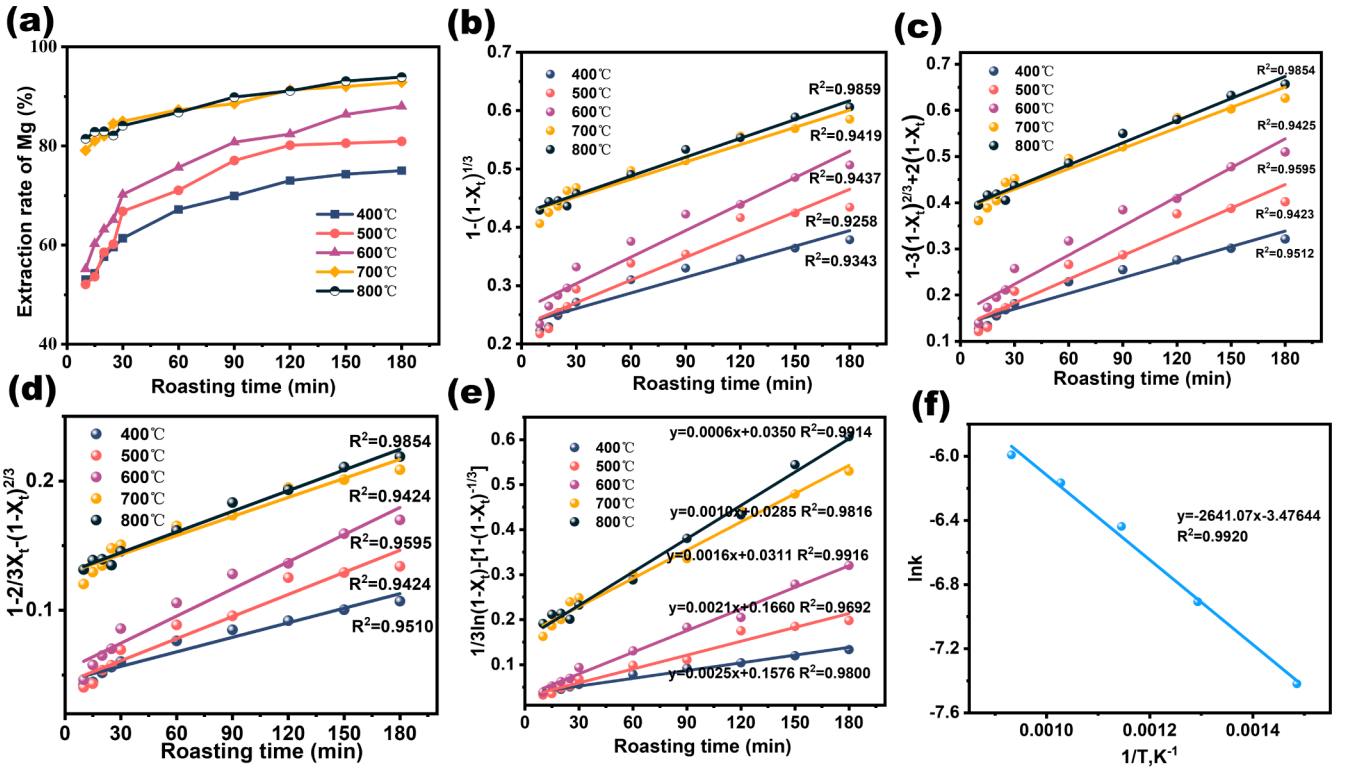


**Figure 8.** Relationship curves of Mg leaching rates and each model with roasting time. (a) Mg leaching rate at various temperatures; (b) $1-(1-X_t)^{1/3}$; (c) $1-3(1-X_t)^{2/3}+2(1-X_t)$; (d) $1-2/3X_t-(1-X_t)^{2/3}$; (e) $1/3\ln(1-X_t)-[1-(1-X_t)^{-1/3}]$; (f) between ln $k$ and $1/T$.

eroded and shrinked during the reaction with concentrated sulfuric acid. In addition, the interaction between CSFT and concentrated sulfuric acid was a solid−liquid heterogeneous reaction. Consequently, the unreacted shrinking core model could be employed to describe the reaction process. In the unreacted shrinking core model, different functions $F(X_t)$



https://doi.org/10.1021/acsomega.4c10942
ACS Omega 2025, 10, 9691−9702

Table 3. $R^2$ Values of the Four Models

| Roasting Time | $1-(1-X_t)^{1/3}$ | $1-3(1-X_t)^{2/3}+2(1-X_t)$ | $1-2/3X_t-(1-X_t)^{2/3}$ | $1/3\ln(1-X_t)-[1-(1-X_t)^{-1/3}]$ |
|---|---|---|---|---|
| 400 °C | 0.9343 | 0.9512 | 0.9510 | 0.9800 |
| 500 °C | 0.9258 | 0.9423 | 0.9424 | 0.9692 |
| 600 °C | 0.9437 | 0.9595 | 0.9595 | 0.9916 |
| 700 °C | 0.9419 | 0.9425 | 0.9424 | 0.9816 |
| 800 °C | 0.9859 | 0.9854 | 0.9854 | 0.9914 |
| average | 0.9463 | 0.9562 | 0.9561 | 0.9828 |

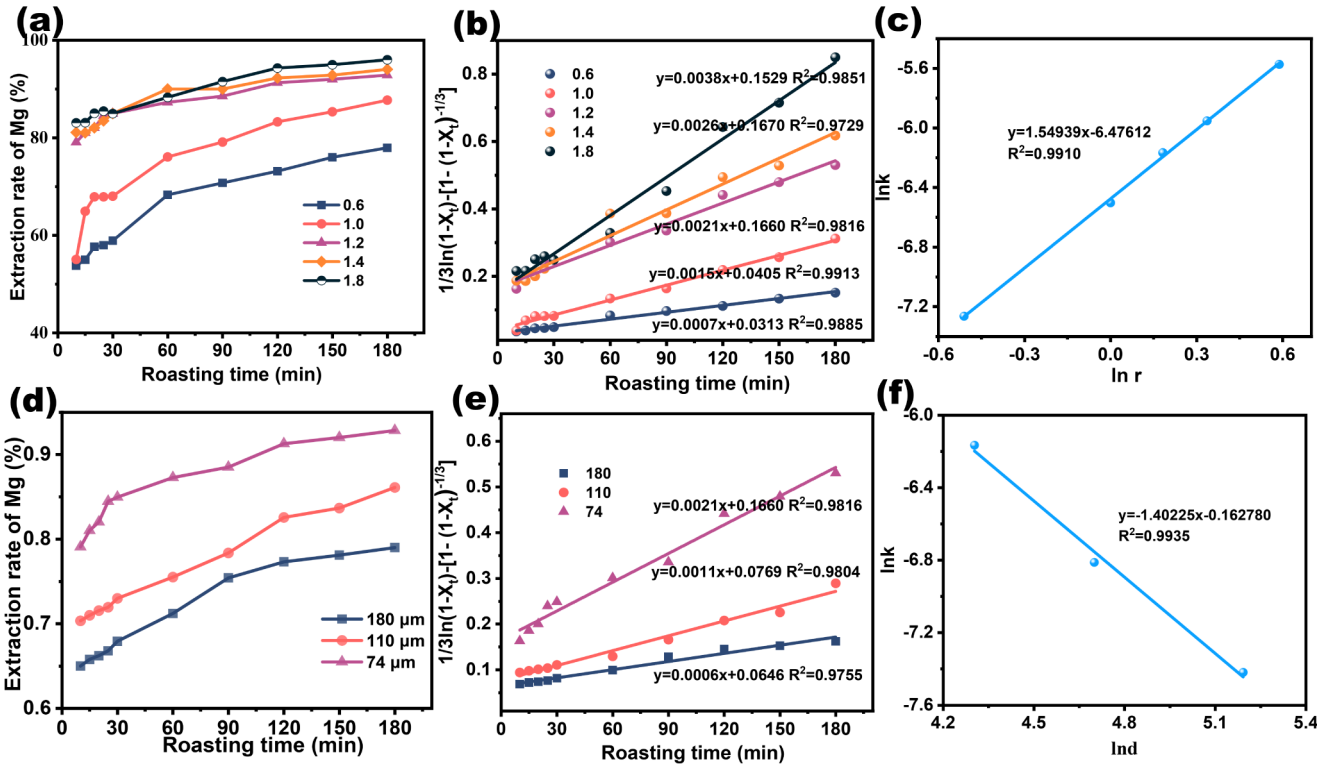


**Figure 9.** Relationship curves of various factors with time, as well as the curves of ln $k$ versus ln $r$ and ln $d$. (a) between Mg leaching rates and roasting time at different acid-to-solid ratios; (b) between $1/3\ln(1-X_t)-[1-(1-X_t)^{-1/3}]$ and roasting time at different acid-to-solid ratios; (c) ln $k$ versus ln $r$; (d) between Mg leaching rates and roasting time at different particle sizes ; (e) between $1/3\ln(1-X_t)-[1-(1-X_t)^{-1/3}]$ and roasting time at different particle sizes; (f) ln $k$ versus ln $d$.

correspond to different resistances controlling the reaction process, as shown in eqs 4−7.[39−40] Equation 4 represents the reaction process controlled by fluid film, eq 5 represents the reaction process controlled by the chemical reaction at the phase interface, eq 6 represents the reaction controlled by the diffusion of the solid product layer, and eq 7 represents the reaction controlled by both product diffusion and interface reaction. The optimal one, eq 8, was determined through experimental fitting, thereby yielding the best function $F(X_t)$. Additionally, eq 9 was established, and the values of $\alpha$, $\beta$, and $E_a$ were calculated through experiments to determine the extent of the influence of each factor.

The leaching rates of Mg in CSFT at temperatures of 400 °C, 500 °C, 600 °C, 700 °C, and 800 °C over roasting time were presented in Figure 8a. Initially, to determine the model of $F(X_t)= kt$ that corresponded to the reaction process, the data within 3 h were linearly fitted according to eqs 4−7, and the results were shown in Figure 8b−f. Comparing the $R^2$ values from Table 3, Model (7) showed the highest linear correlation ($R^2$ > 0.9692, average = 0.9828), leading to the formulation of eq 10.

$$1-3(1-X_t)^{2/3}+2(1-X_t)=k_1t \quad (4)$$

$$1-(1-X_t)^{1/3}=k_2t \quad (5)$$

$$1-2/3X_t-(1-X_t)^{2/3}=k_3t \quad (6)$$

$$1/3\ln(1-X_t)-[1-(1-X_t)^{-1/3}]=k_4t \quad (7)$$

$$F(X_t)=kt \quad (8)$$

$$k=k_5r^{\alpha}d^{\beta}e^{-E_a/RT} \quad (9)$$

$$1/3\ln(1-X_t)-[1-(1-X_t)^{-1/3}]=k_5r^{\alpha}d^{\beta}e^{-E_a/RT}t \quad (10)$$

where $X_t$ represents the leaching rate of Mg at different time (%), $t$ represents the roasting time (min), $k_1$, $k_2$, $k_3$, $k_4$, and $k$ represent reaction rate constants, $k_5$ represents the kinetic constant, $r$ represents the acid-to-solid ratio, $d$ represents the particle size ($\mu$m), $E_a$ is the activation energy of the reaction (J/mol), $R$ is the gas constant, 8.314 J/(mol·K), and $T$ is the reaction temperature ($K$).



https://doi.org/10.1021/acsomega.4c10942
ACS Omega 2025, 10, 9691−9702

*3.4.2. Determination of Parameters in the Evaluation Model.* The activation energy of the reaction can be calculated by using the Arrhenius equation (eq 11).

$$k = A\exp\left(\frac{-E_a}{RT}\right) \tag{11}$$

where $A$ represents the pre-exponential factor, $E_a$ represents the activation energy of the reaction (J/mol), $R$ represents the gas constant, 8.314 J/(mol·K), and $k$ represents the slope of the fitted curves shown in Figure 8e

By taking the natural logarithm of eq 11 and plotting ln $k$ versus $1/T$, we obtained $E_a$ = 21957.8 J/mol and $A$ = 0.03, as depicted in Figure 8f. The $E_a$ can reflect the predominant factors in solid−liquid heterogeneous reactions: $E_a$ above 40 kJ/mol indicates that the reaction rate at the solid−liquid interface is key, while values below 20 kJ/mol suggest that diffusion controls the process. For intermediate $E_a$ (20 to 40 kJ/mol), both the interfacial reaction rate and solid product layer diffusion significantly influence the reaction.[41] Thus, the reaction was primarily influenced by the interfacial reaction rate and solid product layer diffusion, which was consistent with the analysis of influencing factors in Section 3.3.2. In other words, following the addition of concentrated sulfuric acid, thorough mixing with CSFT ensured a robust reaction, thus diminishing the effect of diffusion. Subsequently, as the roasting reaction proceeded, the reduction of sulfuric acid and the accumulation of sulfate and decomposition products on the CSFT surface contributed to a decreased reaction rate.

The leaching rates of Mg in CSFT at acid-to-solid ratios of 0.6, 1.0, 1.2, 1.4, and 1.8 over roasting time are presented in Figure 9a. The leaching rates $X_t$ at various acid-to-solid ratios over time were substituted into the previously derived function $F(X_t)=1/3\ln(1 - X_t) - [1 - (1 - X_t)^{-1/3}]$ and linearly regressed against their respective times. As shown in Figure 9b, the leaching rates of Mg exhibited a significant correlation with this equation. To quantitatively assess the impact of the acid-to-solid ratio on the reaction, temperature and particle size could be treated as constants, thereby reformulating eq 10 into eq 12. Differentiating eq 12 with respect to roasting time ($t$) gives eq 13, where the ratio $d[1/3\ln(1 - X_t) - [1 - (1 - X_t)^{-1/3}]]/dt$ corresponds to the slope ($k$) from the linear fits in Figure 9b. Taking natural logarithms of eq 13 results in eq 14, and plotting (ln $k$) versus (ln $r$) yielded the $\alpha$, with a slope of 1.55 as shown in Figure 9c.

$$1/3\ln(1-X_t) - [1 - (1-X_t)^{-1/3}] = k_6 r^{\alpha} t \tag{12}$$

$$\frac{d[1/3\ln(1-X_t) - [1 - (1-X_t)^{-1/3}]]}{dt} = k_6 r^{\alpha} \tag{13}$$

$$\ln\left[\frac{d[1/3\ln(1-X_t) - [1 - (1-X_t)^{-1/3}]]}{dt}\right] = \ln k_6 + \alpha \ln r \tag{14}$$

The leaching rates of Mg in CSFT at particle sizes of 74, 110, and 180 $\mu$m over varying roasting times were depicted in Figure 9d with a good correlation to the linear fit of the function $F(X_t)=1/3\ln(1-X_t)-[1-(1-X_t)^{-1/3}]$ as shown in Figure 9e. To quantitatively assess the impact of the particle size on the reaction, temperature and acid to solid could be treated as constants, thereby reformulating eq 10− into eq 15.

$$1/3\ln(1-X_t) - [1 - (1-X_t)^{-1/3}] = k_7 d^{\beta} t \tag{15}$$

Using the same approach to determine $\alpha$, we could obtain Figure 9e and subsequently Figure 9f, thereby yielding $\beta$ = −1.40. Thus, eq 10 could be described as eq 16.

$$1/3\ln(1-X_t) - [1 - (1-X_t)^{-1/3}] = k_5 r^{1.55} d^{-1.40} e^{-21957.8/RT} t \tag{16}$$

From the Arrhenius equation, $A$ = 0.03. Substituting $r$ = 1.2 and $d$ = 74 $\mu$m into $k_5\, r^{1.55}\, d^{-1.40} = A$, we could find $k_5$ = 9.36. This led to the quantitative evaluation model, which described the influence of various factors, as shown in eq 17.

$$1/3\ln(1-X_t) - [1 - (1-X_t)^{-1/3}] = 9.36 r^{1.55} d^{-1.40} e^{-21957.8/RT} t \tag{17}$$

The model quantified how roasting temperature, acid-to-solid ratio, and particle size affected the leaching rate $X_t$, with the most significant influence being temperature, followed by the acid-to-solid ratio, and then particle size.

*3.4.3. Validation of the Evaluation Model.* By substituting the Mg leaching rates obtained experimentally into $1/3\ln(1-X_t)$-$[1-(1-X_t)^{-1/3}]$ and the corresponding experimental parameters into $9.36 r^{1.55} d^{-1.40} e^{-21957.8/RT} t$, the comparison in Figure 10 yielded an $R^2$ of 0.9038, demonstrating a strong correlation between predicted and actual values. This model effectively predicted Mg leaching rates and captured the influence of various factors, guiding the optimization of experimental parameters in practical processes.

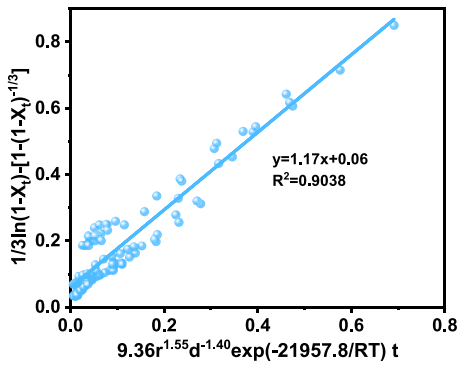


**Figure 10.** Comparison of experimental values with model calculations.

## 4. CONCLUSIONS

In conclusion, this study used concentrated sulfuric acid roasting and subsequent water leaching to extract valuable metals Mg, Cu, and Ni from CSFT, concurrently achieving separation from Fe. Under optimal conditions of a roasting temperature of 700 °C, a roasting time of 120 min, an acid-to-solid ratio of 1.2, and a CSFT particle size of 74 $\mu$m, the extraction rates of Mg, Cu, and Ni reached 91%, 80%, and 87%, respectively. Additionally, the results of ICP and SEM-EDS confirmed that Fe and Si were almost entirely retained in the leaching residue.

Additionally, this study analyzed the effects of roasting temperature, roasting time, acid-to-solid ratio, and CSFT particle size on the extraction of valuable metals, quantifying their impact on the leaching of the primary element Mg. The findings indicated that the influence ranked in order of roasting temperature, acid-to-solid ratio, and particle size. Subsequently,


https://doi.org/10.1021/acsomega.4c10942
ACS Omega 2025, 10, 9691−9702

a dynamic evaluation model depicting the variation of metal leaching rates with these influencing factors was developed, as illustrated in eq 17. Furthermore, fitting the experimental values to the model calculations revealed an $R^2$ value of 0.9038, indicating that the model could accurately reflect the impact of various factors on the experimental outcomes. In practical applications, this model can be used to effectively adjust experimental parameters and swiftly achieve the desired objectives. This work can provide a reference for the efficient extraction of valuable metals from smelting slag and offers guidance for the optimization of metal extraction processes from slag in industrial applications.

## ■ ASSOCIATED CONTENT

### Supporting Information

The Supporting Information is available free of charge at https://pubs.acs.org/doi/10.1021/acsomega.4c10942

Leaching rates of Mg, Fe, Cu, and Ni under different leaching conditions (Figure S1); EDS at different positions in CSFT (Figure S2); SEM−EDS related to (d) of Figure 1 (Figure S3); XRF of CSFT (Table S1); and specific surface area of CSFT with varying particle sizes (Table S2)(PDF)

## ■ AUTHOR INFORMATION


### Corresponding Author

**Xueming Liu** − *School of Environment and Energy, The Key Laboratory of Pollution Control and Ecosystem Restoration in Industry Clusters (Ministry of Education), South China University of Technology, Guangzhou 510006, China; Guangdong Engineering and Technology Research Center for Environmental Nanomaterials, Guangdong Provincial Key Laboratory of Solid Wastes Pollution Control and Recycling, Guangzhou 510006, China; College of Metallurgy and Environment, Central South University, Changsha 410083, China;* orcid.org/0000-0002-4625-2575; Email: esliuxm@scut.edu.cn

### Authors

**Zhuandi Shao** − *School of Environment and Energy, The Key Laboratory of Pollution Control and Ecosystem Restoration in Industry Clusters (Ministry of Education), South China University of Technology, Guangzhou 510006, China; Guangdong Engineering and Technology Research Center for Environmental Nanomaterials, Guangdong Provincial Key Laboratory of Solid Wastes Pollution Control and Recycling, Guangzhou 510006, China*

**Tiantian Wei** − *School of Environment and Energy, The Key Laboratory of Pollution Control and Ecosystem Restoration in Industry Clusters (Ministry of Education), South China University of Technology, Guangzhou 510006, China; Guangdong Engineering and Technology Research Center for Environmental Nanomaterials, Guangdong Provincial Key Laboratory of Solid Wastes Pollution Control and Recycling, Guangzhou 510006, China*

**Xiujuan Zhang** − *School of Environment and Energy, The Key Laboratory of Pollution Control and Ecosystem Restoration in Industry Clusters (Ministry of Education), South China University of Technology, Guangzhou 510006, China; Guangdong Engineering and Technology Research Center for Environmental Nanomaterials, Guangdong Provincial Key Laboratory of Solid Wastes Pollution Control and Recycling, Guangzhou 510006, China*

**Kang Liao** − *School of Environment and Energy, The Key Laboratory of Pollution Control and Ecosystem Restoration in Industry Clusters (Ministry of Education), South China University of Technology, Guangzhou 510006, China; Guangdong Engineering and Technology Research Center for Environmental Nanomaterials, Guangdong Provincial Key Laboratory of Solid Wastes Pollution Control and Recycling, Guangzhou 510006, China*

**Xiaogang Hou** − *Lanzhou Lanshi Zhongke Nanotechnology Co.,Ltd, Lanzhou 730000, China*

**Hong Deng** − *School of Environment and Energy, The Key Laboratory of Pollution Control and Ecosystem Restoration in Industry Clusters (Ministry of Education), South China University of Technology, Guangzhou 510006, China; Guangdong Engineering and Technology Research Center for Environmental Nanomaterials, Guangdong Provincial Key Laboratory of Solid Wastes Pollution Control and Recycling, Guangzhou 510006, China;* orcid.org/0000-0002-6825-8855

**Zhang Lin** − *College of Metallurgy and Environment, Central South University, Changsha 410083, China;* orcid.org/0000-0002-6600-2055

**Liyuan Chai** − *College of Metallurgy and Environment, Central South University, Changsha 410083, China*

Complete contact information is available at: https://pubs.acs.org/10.1021/acsomega.4c10942


### Author Contributions

Z.S.: conceptualization, methodology, investigation, data curation, formal analysis, writing—original draft, and writing—review, and editing; T.W.: supervision, investigation, and writing—original draft; X.Z.: supervision, investigation, and data curation; K.L.: conceptualization, methodology, and supervision; X.H.: supervision, investigation, and methodology; H.D.: funding acquisition, methodology, writing—review, and editing; X.L.: funding acquisition, formal analysis, supervision, writing—review, and editing; Z.L.: formal analysis , supervision, writing—review and editing; L.C.: funding acquisition , formal analysis, supervision, writing—review, and editing.

### Notes

The authors declare no competing financial interest.

## ■ ACKNOWLEDGMENTS

This work was supported by the Foundation for Innovative Research Groups of the National Natural Science Foundation of China (No. 52121004), the National Natural Science Foundation of China (No. 22376070), the 2024 Basic and Applied Basic Research Theme Young Doctoral Program "Kickstart" (No. SL2023A04J00651), and the Guangdong Basic and Applied Basic Research Foundation (2024A1515011395).

## ■ REFERENCES

(1) Lu, K.; Sun, W.; Gao, T.; Li, Z.; Zhao, J.; Cheng, H. Preparation of new copper smelting slag-based mine backfill material and investigation of its mechanical properties. *Constr. Build. Mater.* **2023**, *382*, 131228.

(2) Wang, H.; Zhu, R.; Dong, K.; Zhang, S.; Zhao, R.; Jiang, Z.; Lan, X. An experimental comparison: Horizontal evaluation of valuable metal extraction and arsenic emission characteristics of tailings from

different copper smelting slag recovery processes. *J. Hazard. Mater.* **2022**, *430*, 128493.
(3) Chen, M.; Zhang, J.; Xia, X.; Qi, M.; Yin, J.; Chen, Q. Construction of cobalt sulfide/nickel core-branch arrays and their application as advanced electrodes for electrochemical energy storage. *Electrochim. Acta* **2016**, *195*, 184−191.
(4) Li, B.; Rong, T.; Du, X.; Shen, Y.; Shen, Y. Preparation of $Fe_3O_4$ particles with unique structures from nickel slag for enhancing microwave absorption properties. *Ceram. Int.* **2021**, *47* (13), 18848−18857.
(5) Song, S.; Sun, W.; Wang, L.; Liu, R.; Han, H.; Hu, Y.; Yang, Y. Recovery of cobalt and zinc from the leaching solution of zinc smelting slag. *J. Environ. Chem. Eng.* **2019**, *7* (1), 102777.
(6) Zhou, Y.; Wang, H.; Wang, H.; Dong, K.; Zhu, R.; Jiang, Z.; Wei, G. Mechanism of arsenic distribution and migration during iron extraction by copper slag-steel slag combined reforming: A potential solution to refractory wastes. *J. Cleaner Prod.* **2023**, *420*, 138399.
(7) Shibayama, A.; Takasaki, Y.; William, T.; Yamatodani, A.; Higuchi, Y.; Sunagawa, S.; Ono, E. Treatment of smelting residue for arsenic removal and recovery of copper using pyro-hydrometallurgical process. *J. Hazard. Mater.* **2010**, *181* (1−3), 1016−1023.
(8) Shi, Z. -S.; Ding, Y. -J.; Yin, X. -P.; Liu, B.; Shen, H. -L.; Wu, B. -Y.; Zhao, B. -H.; Han, F. -L.; Ekberg, C.; Zhang, S. -G. Enrichment of Ni-Mo-V via pyrometallurgical reduction from spent hydrogenation catalysts and the multi-reaction mechanism. *Rare Met.* **2023**, *42* (8), 2700−2712.
(9) Priya, J.; Randhawa, N. S.; Hait, J.; Bordoloi, N.; Patel, J. N. High-purity copper recycled from smelter dust by sulfation roasting, water leaching and electrorefining. *Environ. Chem. Lett.* **2020**, *18* (6), 2133−2139.
(10) Kim, B. -S.; Jo, S. -K.; Shin, D.; Lee, J. -C.; Jeong, S. -B. A physico-chemical separation process for upgrading iron from waste copper slag. *Int. J. Miner. Process.* **2013**, *124*, 124−127.
(11) Heo, J. H.; Kim, B. -S.; Park, J. Effect of CaO Addition on Iron Recovery from Copper Smelting Slags by Solid Carbon. *Metall. Mater. Trans. B-Proc. Metall. Mater. Proc. Sci.* **2013**, *44* (6), 1352−1363.
(12) Zhang, J.; Qi, Y. -H.; Yan, D. -L.; Xu, H.-C. A New Technology for Copper Slag Reduction to Get Molten Iron and Copper Matte. *J. Iron Steel Res. Int.* **2015**, *22* (5), 396−401.
(13) Li, Y.; Chen, Y.; Tang, C.; Yang, S.; He, J.; Tang, M. Co-treatment of waste smelting slags and gypsum wastes via reductive-sulfurizing smelting for valuable metals recovery. *J. Hazard. Mater.* **2017**, *322*, 402−412.
(14) Geng, C.; Wang, H. -J.; Hu, W. -T.; Li, L.; Shi, C. -S. Recovery of iron and copper from copper tailings by coal-based direct reduction and magnetic separation. *J. Iron Steel Res. Int.* **2017**, *24* (10), 991−997.
(15) Yao, G.; Guo, Q.; Li, Y.; Xu, Z.; Han, Z.; He, M.; Qi, T. An innovation technology for recovering silver and valuable metals from hazardous zinc leaching residue through direct reduction. *Miner. Eng.* **2022**, *188*, 107857.
(16) Dang, H.; Li, N.; Chang, Z.; Wang, B.; Zhan, Y.; Wu, X.; Liu, W.; Ali, S.; Li, H.; Guo, J.; et al. Lithium leaching via calcium chloride roasting from simulated pyrometallurgical slag of spent lithium ion battery. *Sep. Purif. Technol.* **2020**, *233*, 116025.
(17) Guo, X.; Li, D.; Park, K. -H.; Tian, Q.; Wu, Z. Leaching behavior of metals from a limonitic nickel laterite using a sulfation-roasting-leaching process. *Hydrometallurgy* **2009**, *99* (3−4), 144−150.
(18) Zhao, Z.; Li, H.; Wang, C.; Xing, P. Transformation mechanism and selective leaching of nickel and cobalt from limonitic laterite ore using sulfation-roasting-leaching process. *J. Cleaner Prod.* **2024**, *445*, 141327.
(19) Li, G.; Cheng, H.; Chen, S.; Lu, X.; Xu, Q.; Lu, C. Mechanism of $Na_2SO_4$ Promoting Nickel Extraction from Sulfide Concentrates by Sulfation Roasting-Water Leaching. *Metall. Mater. Trans. B-Proc. Metall. Mater. Proc. Sci.* **2018**, *49* (3), 1136−1148.
(20) Sun, Q.; Cheng, H.; Mei, X.; Liu, Y.; Li, G.; Xu, Q.; Lu, X. Efficient Synchronous Extraction of Nickel, Copper, and Cobalt from Low-Nickel Matte by Sulfation RoastingWater Leaching Process. *Sci. Rep.* **2020**, *10* (1), 9916.
(21) Mu, W.; Cui, F.; Huang, Z.; Zhai, Y.; Xu, Q.; Luo, S. Synchronous extraction of nickel and copper from a mixed oxide-sulfide nickel ore in a low-temperature roasting system. *J. Cleaner Prod.* **2018**, *177*, 371−377.
(22) Cui, F.; Mu, W.; Wang, S.; Xin, H.; Xu, Q.; Zhai, Y. A Sustainable and Selective Roasting and Water-Leaching Process to Simultaneously Extract Valuable Metals from Low-Grade Ni-Cu Matte. *JOM* **2018**, *70* (10), 1977−1984.
(23) Xing, P.; Ma, B. -Z.; Zeng, P.; Wang, C. -Y.; Wang, L.; Zhang, Y. -L.; Chen, Y. -Q.; Wang, S.; Wang, Q. -Y. Deep cleaning of a metallurgical zinc leaching residue and recovery of valuable metals. *Int. J. Miner. Metall. Mater.* **2017**, *24* (11), 1217−1227.
(24) Chen, S.; Feng, Z.; Wang, M.; Zhao, L.; Yu, Z.; Xia, C.; Huang, X. Leaching kinetic study of sulfuric acid roasted mixed-type rare earth concentrate for reducing the solid-waste production and chemical consumption. *J. Cleaner Prod.* **2020**, *260*, 120989.
(25) Fan, J.; Wang, G.; Li, Q.; Yang, H.; Xu, S.; Zhang, J.; Chen, J. W.; Wang, R. Extraction of tellurium and high purity bismuth from processing residue of zinc anode slime by sulfation roasting-leaching-electrodeposition process. *Hydrometallurgy* **2020**, *194*, 105348.
(26) Zhang, X. F.; Tan, X. M.; Li, C.; Yi, Y. J.; Liu, W. Z.; Zhang, L. Z. Energy-efficient and simultaneous extraction of lithium, rubidium and cesium from lepidolite concentrate via sulfuric acid baking and water Cheek Tor leaching. *Hydrometallurgy* **2019**, *185*, 244−249.
(27) Madakkaruppan, V.; Pius, A.; Sreenivas, T.; Giri, N.; Sarbajna, C. Influence of microwaves on the leaching kinetics of uraninite from a low grade ore in dilute sulfuric acid. *J. Hazard. Mater.* **2016**, *313*, 9−17.
(28) Peng, H.; Guo, J.; Zheng, X.; Liu, Z.; Tao, C. Leaching kinetics of vanadium from calcification roasting converter vanadium slag in acidic medium. *J. Environ. Chem. Eng.* **2018**, *6* (4), 5119−5124.
(29) Ye, J.; Chen, J.; Luo, K.; Yan, F.; Zhang, W.; Ren, X.; Li, J.; Rong, H. The leaching model and leaching kinetics of lithium slag in alkaline solution. *Constr. Build. Mater.* **2024**, *432*, 136642.
(30) Xiao, W.; Li, Y.; Zhao, Z.; Liu, X. Leaching kinetics of low nickel matte in an aqueous solution of sulfuric acid saturated with $FeSO_4$ and $NiSO_4$. *Sep. Purif. Technol.* **2021**, *276*, 119375.
(31) Li, M.; Zheng, S.; Liu, B.; Du, H.; Dreisinger, D.; Tafaghodi, L.; Zhang, Y. The leaching kinetics of cadmium from hazardous Cu-Cd zinc plant residues. *Waste Manage.* **2017**, *65*, 128−138.
(32) Shi, G.; Liao, Y.; Su, B.; Zhang, Y.; Wang, W.; Xi, J. Kinetics of copper extraction from copper smelting slag by pressure oxidative leaching with sulfuric acid. *Sep. Purif. Technol.* **2020**, *241*, 116699.
(33) Guemuessoy, A.; Basyigit, M.; Kart, E. Economic potential and environmental impact of metal recovery from copper slag flotation tailings. *Resour. Policy.* **2023**, *80*, 103232.
(34) Siriwardane, R. V.; Poston, J. A., Jr.; Fisher, E. P.; Shen, M. -S.; Miltz, A. L. Decomposition of the sulfates of copper, iron (II), iron (III), nickel, and zinc: XPS, SEM, DRIFTS, XRD, and TGA study. *Appl. Surf. Sci.* **1999**, *152* (3−4), 219−236.
(35) Scheidema, M. N.; Taskinen, P. Decomposition Thermodynamics of Magnesium Sulfate. *Ind. Eng. Chem. Res.* **2011**, *50* (16), 9550−9556.
(36) Ozer, M.; Acma, E.; Atesok, G. Sulfation roasting characteristics of copper-bearing materials. *Asia-Pac. J. Chem. Eng.* **2017**, *12* (3), 365−373.
(37) Cavani, F.; Trifirò, F.; Vaccari, A. HYDROTALCITE-TYPE ANIONIC CLAYS: PREPARATION, PROPERTIES AND APPLICATIONS. *Catal. Today* **1991**, *11* (2), 173−301.
(38) Rodrigues, A. C. C.; Henriques, C. A.; Monteiro, J. L. F. Influence of Ni content on physico-chemical characteristics of Ni, Mg, Al-Hydrotalcite like compounds. *Mater. Res.* **2003**, *6* (4), 563−568.
(39) Chen, D. -S.; Zhao, L. -S.; Qi, T.; Hu, G. -P.; Zhao, H. -X.; Li, J.; Wang, L. -N. Desilication from titanium-vanadium slag by alkaline leaching. *Trans. Nonferrous Met. Soc. China* **2013**, *23* (10), 3076−3082.


https://doi.org/10.1021/acsomega.4c10942
*ACS Omega* 2025, 10, 9691−9702

(40) Dickinson, C. F.; Heal, G. R. Solid-liquid diffusion controlled rate equations. *Thermochim. Acta* **1999**, *340-341*, 89−103.
(41) Gharabaghi, M.; Irannajad, M.; Azadmehr, A. R. Leaching kinetics of nickel extraction from hazardous waste by sulphuric acid and optimization dissolution conditions. *Chem. Eng. Res. Des.* **2013**, *91* (2), 325−331.



https://doi.org/10.1021/acsomega.4c10942
*ACS Omega* 2025, 10, 9691−9702